GEOPHYSICS, VOL. 87, NO. 2 (MARCH-APRIL 2022); P. MR49–MR62, 13 FIGS., 3 TABLES.
10.1190/GEO2020-0918.1

DOI:10.1190/geo2020-0918.1

Using rock-physics models to validate rock composition from multimineral log analysis

Liwei Cheng[1], Manika Prasad[1], Reinaldo J. Michelena[2], Ali Tura[1], Shamima Akther[3], Petar Vladov Angelov[3], and Rao Narhari Srinivasa[3]

ABSTRACT

Multimineral log analysis is a quantitative formation evaluation tool for geologic and petrophysical reservoir characterization. Rock composition can be estimated by solving equations that relate log measurements to the petrophysical endpoints of minerals and fluids. Due to errors in log data and uncertainties in petrophysical endpoints of constituents, we have used effective medium models from rock physics as additional independent information to validate or constrain the results. We examine the Voigt-Reuss (VR) bound model, self-consistent approximation (SCA), and differential effective medium (DEM). The VR bound model provides the first-order quality control of multimineral results. We first show a conventional carbonate reservoir study with intervals in which the predicted effective medium models from multimineral results are inconsistent with measured elastic properties. We use the VR bound model as an inequality constraint in multimineral analysis for plausible alternative solutions. The SCA and DEM models provide good estimates in low-porosity intervals and imply geologic information for porous intervals. Then, we present a field case of the Bakken and Three Forks formations. A linear interpolation of the VR bound model helps validate multimineral results and approximate the elastic moduli of clay. There are two major advantages to using our new method: (1) Rock-physics effective medium models provide independent quality control of petrophysical multimineral results and (2) multimineral information leads to realistic rock-physics models.

INTRODUCTION

Multimineral log analysis quantifies the volume fractions of minerals and fluids (collectively as constituents) at every depth for reservoir characterization in the absence of elemental logs. Petrophysical parameters such as porosity, lithology, and fluid saturation can be related to logging tool measurements through theoretical equations. Multimineral log analysis (multimineral analysis hereafter) is particularly valuable in complex lithology and depositional systems. Mayer and Sibbit (1980) optimize petrophysical parameters through the steepest-descent technique that minimizes the misfits between measured logs and their theoretical values. Quirein et al. (1986) use quadratic minimizations with linearized response equations, which significantly reduce computation time. For a better model in thinly bedded formations, nonlinear responses of nuclear logs are incorporated in multimineral analysis by Heidari et al. (2012).

The typical input data of multimineral analysis are triple- or quad-combo logging sets. A triple-combo logging set includes gamma-ray (GR), resistivity (RT), neutron porosity (NPHI), photoelectric effect (PEF), and bulk density (RHOB) measurements. A quad-combo logging set implements an additional sonic tool to measure compressional slowness (DTC) and shear slowness (DTS, when using a dipole source) along the wellbore direction. The measured logs are related to the composition of saturated rocks through a set of theoretical equations. Multimineral analysis involves an inverse problem that minimizes misfit between log measurements and reconstructed theoretical log measurements for rock composition. Due to several sources of uncertainty, the

Manuscript received by the Editor 16 December 2020; revised manuscript received 29 October 2021; published ahead of production 28 November 2021; published online 21 January 2022.
[1]Colorado School of Mines, Department of Geophysics, Golden, Colorado 80401-1887, USA. E-mail: lcheng@mines.edu (corresponding author); mprasad@mines.edu; alitura@mines.edu.
[2]SeisPetro Geosoftware, LLC., Littleton, Colorado 80120, USA. E-mail: michelena@seispetro.com.
[3]Kuwait Oil Company, Ahmadi, 61008, Kuwait. E-mail: SAkther@kockw.com; PAngelov@kockw.com; Nsrao@kockw.com.

inversion result is commonly cross-checked with other available information, such as core measurements, mud logs, and local geologic knowledge. Note that multimineral analysis most often focuses on determining rock composition and does not consider the texture of the rock. Therefore, solutions from conventional multimineral analysis may violate rock-physics theories and make them unrealistic in terms of rock physics. Heidari et al. (2012) discuss the possibility of implementing the effective medium model in multimineral analysis workflow to validate the results.

In current practice, sonic logs are embedded in multimineral analysis through empirical slowness or velocity equations, most commonly using the Wyllie time-average (WTA) (Wyllie et al., 1956) or the Raymer-Hunt-Gardner (Raymer et al., 1980) velocity-porosity relations. However, those relations are heuristic and may only be valid in certain rock settings. For instance, the WTA may only apply to low-to-medium porosity sandstones (Dvorkin and Nur, 1998) and includes no information about pore shape and texture. The use of inappropriate velocity-porosity models may lead to erroneous interpretations (Kittridge, 2014). This paper incorporates effective medium models in multimineral analysis and provides a more general rock-physics evaluation.

This paper uses quad-combo logging sets for multimineral analysis and uses the measured elastic moduli derived from density and sonic logs to validate the results. The measured elastic properties are compared with the theoretical effective medium models predicted from the multimineral results. Effective medium models used in the paper are the Voigt-Reuss (VR) bound model, self-consistent approximation (SCA), and differential effective medium (DEM). A violation occurs when the measured elastic modulus is greater than the upper limit or smaller than the lower limit predicted from the effective medium models. Any interval with a violation may require reevaluating the multimineral model and may be imposed with constraints in the inversion to search for alternative solutions.

In the following sections, we first introduce the concepts and workflow of multimineral analysis. Then, we explain the effective medium models that are used in this paper. Next, we apply multimineral analyses to a deep Jurassic carbonate formation in North Kuwait and the Bakken Shale Formation in North Dakota, USA. We demonstrate how to implement inequalities to constrain the inverse problem if violations are present and cross-check multimineral results with effective medium models even if there is no violation. RHOB and dipole sonic logs are available in both cases. We can evaluate the multimineral model's plausibility by analyzing the effective medium models derived from the multimineral results.

The compositional model used in this paper is shown in Figure 1, as the constituents include clay and nonclay minerals as the solid phase and fluids as the liquid phase in the pore space.

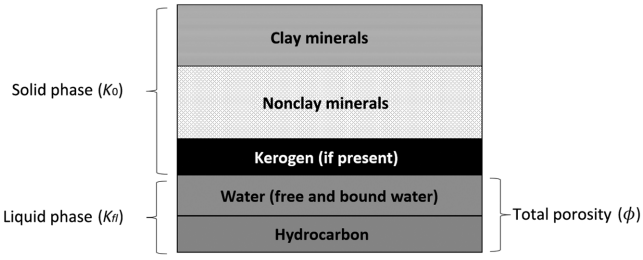

Figure 1. The compositional model assumed in this paper.

MULTIMINERAL ANALYSIS

In a monomineralic rock with a single phase of fluid, linear interpolation between two endpoints of the mineral and fluid can provide estimates of mineral and pore volumes. However, the subsurface is composed of multiple minerals and fluids. A multimineral problem requires multiple measurements and equations that relate the unknown composition to the measurements. At every depth, multimineral analysis optimizes a solution of rock composition that appropriately matches all input measurements. The first step of multimineral analysis is to select constituents that compose the saturated rock. Core analysis assisted by mud logs is a common approach to determine lithology. Core measurements, such as X-ray diffraction (XRD) and X-ray fluorescence (XRF), help determine the most probable constituents and provide quantitative quality control for multimineral results.

After determining the rock constituents, we use the mixing law that assumes linear relationships between log responses and the petrophysical endpoints of constituents weighted by their volume fractions for forward simulation (Quirein et al., 1986; Mitchell and Nelson, 1988; Doveton, 1994; Rabaute et al., 2003). We assume a dispersed shale model for RT if clay minerals are present. We use Archie (1942) to linearize RT for near-wellbore square root conductivity (CX) when the porosity and saturation exponents are assumed to be two (Doveton, 1994). The total response of CX can be expressed as

$$CX = \sum_{i}^{N} CX_i m_i, \tag{1}$$

where CX_i is the square root conductivity of the ith constituent and is assumed to be zero for nonclay minerals and hydrocarbons and m_i is the volume fraction of the ith constituent. We assume that the deep conductivity log represents uninvaded zones. In the absence of gas in the formation, the theoretical log response for each depth can be expressed as

$$d = Gm, \tag{2}$$

where d is the log response and G is an $M \times N$ matrix of constituent petrophysical endpoints (where M is the number of independent logging tools and N is the number of constituents). For a triple-combo logging set with a litho-density tool (LDT), the petrophysical endpoint matrix G can be expressed by

$$G = \begin{bmatrix} \mathrm{GR}_1 & \mathrm{GR}_2 & \dots & \mathrm{GR}_i \\ Cx_1 & Cx_1 & \dots & Cx_i \\ \rho_{b1} & \rho_{b2} & \dots & \rho_{bi} \\ \phi_{N1} & \phi_{N2} & \dots & \phi_{Ni} \\ U_1 & U_2 & \dots & U_i \\ 1 & 1 & \dots & 1 \end{bmatrix}, \tag{3}$$

where GR_i is the gamma ray, CX_i is the square root conductivity, ρ_{bi} is the bulk density, ϕ_{Ni} is the neutron porosity, and U_i is the volumetric cross-section endpoints of the ith constituent. The multimineral analysis uses the linear superposition of the volumetric cross section (U) derived from PEF and RHOB. The m is an N by one vector of volume fractions of constituents, given by

DOI:10.1190/geo2020-0918.1

$$m = [m_1\ m_2 \ldots\ m_i]^T, \tag{4}$$

where T denotes a matrix transpose. The log responses are given by

$$d = [\mathrm{GR}\ CX\ \rho_b\ \phi_N\ U\ 1]^T. \tag{5}$$

The ones in equations 3 and 5 represent the unity equation ($\sum_{i=1}^{N} m_i = 1$), which states that the sum of all volume fractions should equal one.

This paper uses deterministic inversion and stochastic Monte Carlo simulations for multimineral analysis. The deterministic inversion is solved at every depth by the L-2 norm solution of equation 2 to minimize the objective function given by

$$\min_m \|Gm - d\|_2^2, \tag{6}$$

subject to

$$0 \le m_i \le 1. \tag{7}$$

Equation 6 is normalized by the standard deviation of each measurement (Mitchell and Nelson, 1988). The constraint of equation 7 prohibits unrealistic solutions.

In addition to data errors, the individual endpoint value in the matrix of constituent petrophysical endpoints (G) plays a significant role (Michelena et al., 2020). Total porosity (ϕ), for example, can be generally approximated by using the density-porosity formula, given by $\phi = (\rho_b - \rho_f)/(\rho_m - \rho_f)$, where ρ_m is matrix density and ρ_f is fluid density, due to the clear separation between the density of fluid (approximately 1 g/cm^3) and the density of matrix (e.g., quartz: 2.65 g/cm^3 or calcite: 2.71 g/cm^3). However, when other minerals with similar petrophysical endpoints are present, the uncertainty of solution is higher, and the resultant composition estimates may be erroneous. Therefore, we also use the stochastic Monte Carlo simulations to assess the uncertainty of solutions due to errors in data and similarity in petrophysical endpoints. Markov chain Monte Carlo (MCMC) simulations in the Bayesian framework provide a means by which uncertainties in the data and formula can be translated into uncertainties in the simulated results. The solutions found by MCMC simulations are shown in posterior probability functions at every depth. The multimineral results from the deterministic and stochastic methods are consistent. However, MCMC simulations provide associated uncertainties with many plausible realizations that fit the data within the given data misfit. More details about the MCMC simulations used in this paper can be found in Appendix A.

Note that a multimineral result with an acceptable data misfit may not accurately quantify the formation's composition. Instead, it is a solution consistent with the input logs and the choice of constituents and their petrophysical endpoints. Multimineral results are recommended to be reconciled with other available information, such as mud logs, core data, and local knowledge, by iteratively altering tool responses. This paper presents using effective medium models from rock-physics analysis to validate or constrain multimineral results.

EFFECTIVE MEDIUM THEORY

Triple- or quad-combo log data are the standard inputs for multimineral analysis. Triple-combo log data respond to the aggregate responses of either gamma-ray (GR, RHOB, and PEF) or neutrons (NPHI) from formations and are sensitive to rock composition. However, the logs, except RT through Archie's equation, do not contain the geometric information of the rock. Geometric information includes pore shapes, cementation, and texture, which is critical to rock-physics analysis. Therefore, multimineral analysis using triple-combo log data may result in unrealistic solutions that violate rock-physics theories.

When quad-combo log data are available, the sonic slowness or velocity log is commonly embedded as constraining data through empirical relations, for example, WTA, to assist the inversion of the rock composition. However, those empirical relations are heuristic and cannot be justified theoretically (Mavko et al., 2009). Implementing inappropriate relations that do not account for geometric details may lead to erroneous interpretations.

Instead of using empirical relations, we propose incorporating the effective medium theory to cross-check or constrain the multimineral results. The effective medium theory uses theoretical models to predict the elastic properties of a rock. Effective medium models require information about (1) the rock composition, which can be solved by multimineral analysis, and (2) the elastic moduli of constituents, which can be obtained from laboratory experiments. Thus, one may evaluate and improve the multimineral results in an iterative approach by implementing effective medium models. Table 1 lists the elastic moduli used in this paper.

We demonstrate our method by comparing the measured bulk modulus log with effective medium models predicted from multimineral results. The effective bulk modulus of the saturated rock (K_{sat}) is given by

$$K_{\mathrm{sat}} = \rho_b \left(V_{\mathrm{P}}^2 - \frac{4}{3} V_{\mathrm{S}}^2 \right), \tag{8}$$

where ρ_b is bulk density, V_{P} is compressional-wave velocity, and V_{S} is shear-wave velocity. Assuming that the rock is isotropic, equation 8 computes the bulk modulus log from density and slowness logs. If the rock is transversely isotropic, it is ideal to use velocity measurements from different directions with anisotropic equations

Table 1. Elastic moduli of constituents used in this paper; S- and P-wave moduli are only used in the Middle Marrat analysis.

Constituent	Bulk modulus (GPa)	Shear modulus (GPa)	P-wave modulus (GPa)	Reference
Anhydrite	62.1	33.6	106.9	Rafavich et al. (1984)
Calcite	74.8	30.6	115.5	Dandekar (1986)
Dolomite	94.9	45.0	154.6	Humbert and Plieque (1972)
Clay	12.0	6.0	20	Vanorio et al. (2003)
Kerogen	5.0	—	—	Yan and Han (2013)
Quartz	37.0	—	—	Carmichael (1989)
Water	2.2	0	2.2	Mavko et al. (2009)
Oil	1.6	0	0.8	—

DOI:10.1190/geo2020-0918.1

(see King, 1969) to compute the effective bulk modulus. However, due to the limitations of quad-combo logging, we use equation 8 to approximate the effective bulk modulus for common practice. Note that the vertical resolution of the bulk modulus log is subject to the vertical resolution of the DTS log, which is generally lower than other logs used in multimineral analysis. Walker et al. (2019) show that for an 8.5 in. borehole with a 15% velocity contrast, beds with less than 3 ft thickness are not resolvable. For formations with thinly bedded layers, inconsistent vertical resolution should be taken into account in the analysis.

We present results of three different effective medium models: the VR bound model and two inclusion models, the SCA and DEM, compared with the bulk modulus log.

First, the VR bound model defines the extreme upper and lower limits of effective elastic moduli for a multimineral rock when only the rock composition and elastic moduli of constituents can be specified. The Voigt and Reuss bounds are the arithmetic and harmonic average of constituent elastic moduli, respectively. The Voigt (1889) average in terms of bulk modulus (K_V) can be expressed as

$$K_V = \sum_{i=1}^{N} K_i m_i, \tag{9}$$

where K_i is the bulk modulus of the ith constituent and N is the total number of constituents. The Reuss average (Reuss, 1929) in terms of the bulk modulus (K_R) is given by

$$\frac{1}{K_R} = \sum_{i=1}^{N} \frac{m_i}{K_i}. \tag{10}$$

The Reuss average defines a fluid-supported suspension system with a zero dry frame bulk modulus. Therefore, the effective bulk moduli of consolidated rocks should lie somewhere above the Reuss bound.

Hashin-Shtrikman (HS) (Hashin and Shtrikman, 1963) bounds are another viable bound model to incorporate in multimineral analysis. HS bounds define the narrowest possible range without specifying anything about the geometries of the constituents (Mavko et al., 2009) and assume that the rock is isotropic. However, caution should be taken that there are extreme cases in which the effective elastic moduli can be outside the ranges predicted by HS bounds. Thus, for the bound model, we focus our application on VR averages.

The underlying assumption of the VR bound model is that each constituent is isotropic and linearly elastic. The composite may be anisotropic because VR averages correspond to the most extreme cases of transverse isotropy and are independent of geometry at a given composition (Hill, 1964). The effective elastic moduli of a multimineral rock should fall between the VR bounds (Mavko et al., 2009). Sone and Zoback (2013) examine various shale-gas reservoir rocks, and their laboratory data generally conform to the theory and lie within the VR bounds.

When the measurement is inside the VR bounds, the linear interpolation between the bounds can be used as an estimation of rock texture (Marion and Nur, 1991) given by

$$w = (K_{\text{sat}} - K_R)/(K_V - K_R), \tag{11}$$

where w is a weighting factor estimated from the Voigt and Reuss averages. The difference in the weighting factor may represent the distinct pore space, rock fabric, and geometry of the rock. Note that $w > 1$ indicates a violation in the Voigt average and $w < 0$ represents a violation in the Reuss average.

The VR bound model is valid for other elastic moduli, such as S- and P-wave moduli. Therefore, we also present an application in the VR bound model that uses P-wave modulus (M_{sat}) where $M_{\text{sat}} = \rho_b V_P^2$ when the DTS log is absent or noisy. In theory, the P-wave modulus log has a higher vertical resolution (approximately 2 ft) and is less affected by noise than the bulk modulus log.

The VR bound model establishes the upper and lower limits given the composition and elastic moduli of the constituents. However, the large contrast in moduli between solid and fluid components can mask minor differences between mineral moduli of the solids. Therefore, we use the second set of effective medium models to cross-check the rock composition further.

In addition to the rock composition and elastic moduli of the constituents, the SCA and DEM models need additional specifications in the pore aspect ratio (AR) of inclusions to predict more realistic effective elastic moduli. In SCA, rock constituents are selected to be load-bearing based on their volume fractions. At high porosity, greater than 60%, Berryman (1980) shows that the fluid phase becomes load-bearing. Using the same argument, Das and Batzle (2009) point out that the medium is biconnected between 40% and 60% porosity in the SCA formulation. Berryman (1980) estimates effective elastic moduli by changing inclusion shapes through AR specification. For example, AR = 0.01 represents penny-shaped, and AR = 1 indicates spherical inclusions, cracks, and pores, respectively, if inclusions represent pore space. The SCA does not identify any specific host material, but it treats the composite as an aggregate of all the constituents (Mavko et al., 2009). However, the host rock is assumed to be homogeneous, isotropic, and linearly elastic with randomly oriented ellipsoidal pore inclusions.

The DEM allows for the calculation of elastic properties by assigning one constituent as the host. In a two-phase medium, the composition is changed by incrementally adding inclusions of one phase to the matrix host phase (Zimmerman, 1990; Berryman et al., 2002). In the DEM model, the inclusions/cracks are isolated in the host matrix and represent a no-flow condition. In our approach, we develop the following workflow for calculating DEM:

Table 2. Petrophysical endpoints used for the Middle Marrat Formation.

Constituent	GR (API)	Conductivity (S/m)	Density (g/cm^3)	Neutron porosity (fraction)	Volumetric cross section (barns/cm^3)
Anhydrite	5	0	2.98	−0.02	14.9
Calcite	5	0	2.71	0	13.8
Dolomite	10	0	2.87	0.03	9.1
Clay	80	0.3	2.79	0.3	8.5
Water	0	9	1.0	1.0	0.4
Oil	0	0	0.8	0.95	0.1

1) Estimate the constituent volume fractions from multimineral analysis.
2) Use the Voigt-Reuss-Hill average (Hill, 1952) to compute the elastic properties of the matrix phase.
3) Use Wood's formula (Wood, 1955) for the elastic properties of the inclusions.
4) Calculate elastic moduli using the DEM model with the specified AR.

Theoretically, the inclusion models provide good approximations for low inclusion density/porosity (Saxena et al., 2018), and we use AR = [0.01, 1] as lower and upper bounds for the SCA and DEM.

Figure 2 illustrates a crossplot of effective medium models of a calcite-water composite in bulk modulus. The VR bounds define the uppermost and lowermost limits of effective elastic moduli. SCA and DEM narrow the prediction of effective bulk modulus by specifying AR = [0.01, 1], respectively. Note that we only focus on application to the rocks whose porosity is less than their critical porosity. The modified Voigt average and percolation in DEM are not implemented in our models.

The proposed multimineral analysis workflow is illustrated in Figure 3. We suggest an additional evaluation of effective medium models at every depth after the conventional calibration process to validate the results. In addition to selecting different constituents and iterating their petrophysical endpoints and tool responses, postinversion calibration can be made by enabling inequality constraints in the inverse process when violations are present. We show our workflow in the following section with two field examples.

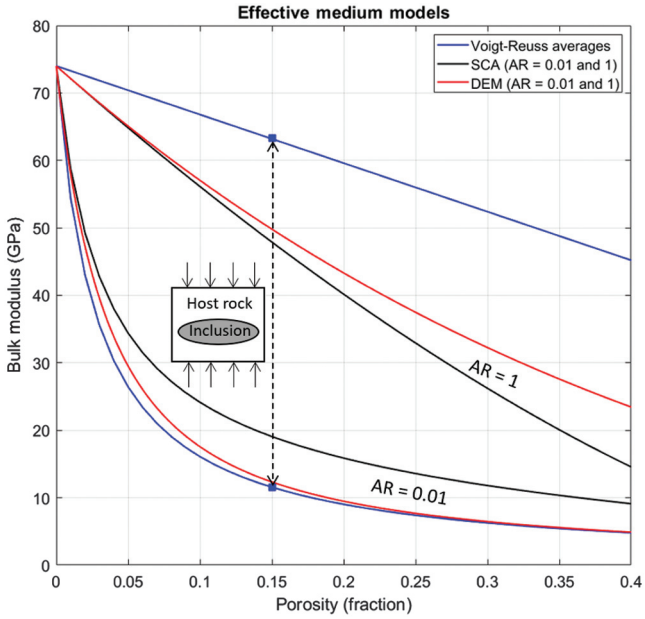

Figure 2. Effective medium models for a calcite-water composite in bulk modulus. The Voigt and Reuss averages define the most extreme cases in elastic behaviors for a composite rock. The SCA and DEM are inclusion models that use the inclusions' AR to predict effective moduli of a composite rock; AR = 0.01 (penny-shaped) and AR = 1 (spherical) of the SCA and DEM are shown in black and red curves, respectively.

FIELD EXAMPLES

To demonstrate our method in multimineral analysis that incorporates the effective medium models, we present two field cases: the conventional Middle Marrat Formation in North Kuwait and the unconventional Bakken and Three Forks formations in North Dakota, USA. No empirical slowness/velocity relations are embedded, and bulk modulus logs are used as additional information in analyses. We show multimineral solutions from MCMC simulations and deterministic inversion for the two cases. In addition to obvious geologic differences, the examples in the two areas help illustrate how to use effective medium models in evaluating the results.

Middle Marrat Formation, North Kuwait

The first field example is a carbonate reservoir in North Kuwait, where the Marrat Formation was deposited on a vast carbonate-evaporite platform during the early Jurassic time (Murris, 1980). The Marrat Formation is conventionally divided into upper, middle, and lower units, separated by maximum flooding surfaces. In this field example, we focus on the Middle Marrat unit (MMR), the main producing unit. The porosity can be up to 25%. The MMR consists of a sequence of dense micritic limestones with subordinate wackstones, packstones, and oolitic grainstones, frequently with anhydrite, dolomite, and rare clay (Alsharhan et al., 2014). It is critical to correctly estimate the volumes of iterative anhydrite between porous intervals for reservoir development. The anhydrite volume may impact the vertical connectivity of different flow zones.

According to the mud logs and production data, we select calcite, dolomite, anhydrite, clay, water, and light oil as the constituents of the rocks in the interval of interest. Available well logs are GR, RT, RHOB, NPHI, U, DTC, and DTS. The petrophysical endpoints of constituents used in this example are listed in Table 2. The inverse problem is even-determined because the number of equations

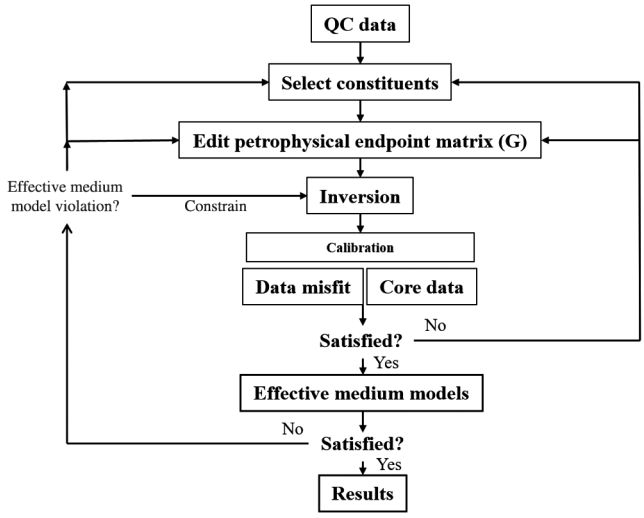

Figure 3. The proposed workflow for multimineral analysis incorporating effective medium models. The evaluation of effective medium models is added to the postinversion calibration. When violations of effective medium models are present, in addition to reviewing the constituents and their petrophysical endpoints, inequality constraints can be imposed on the inverse process.

equals the number of unknown constituent volume fractions. DTC and DTS are not used in the inversion, but they are used to compute the bulk modulus log.

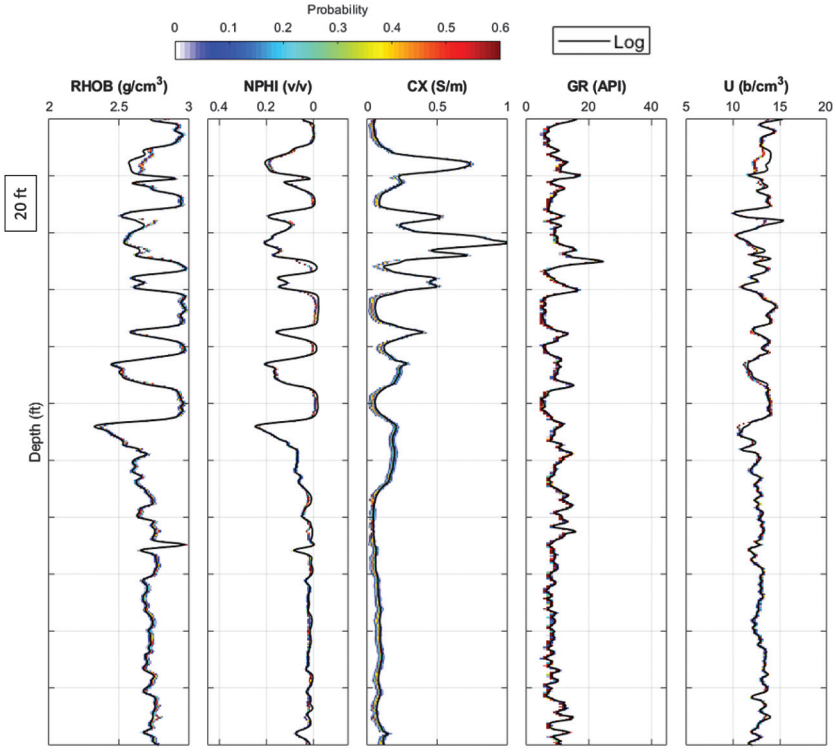

Figure 4. The input logs and reconstructed logs from plausible realizations from MCMC simulations for the Middle Marrat Formation. The reconstructed logs are shown in the posterior probability functions at every depth. The color scheme represents the probability.

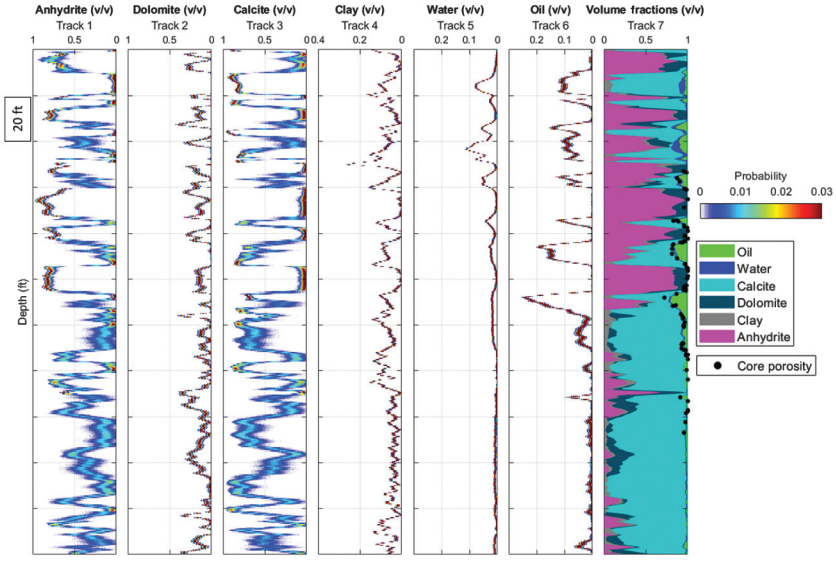

Figure 5. The posterior probability functions of constituent volume fractions (tracks 1–6) from MCMC simulations and the deterministic result (track 7). The core porosity measurements are compared with the multimineral result. Anhydrite and calcite exhibit high uncertainties in volume fraction due to the similarity in their petrophysical endpoints.

Stochastic and deterministic multimineral analyses are performed. In total, 5% of summed data misfits are determined acceptable for MCMC simulations. Figure 4 shows the input logs and reconstructed logs in probability from plausible realizations from the MCMC simulations, and the two have good matches. Tracks 1–6 of Figure 5 show the posterior probability functions of constituent volume fractions. The uncertainties in anhydrite and calcite are higher than other constituents, mainly due to the similarity in their petrophysical endpoints. Track 7 of Figure 5 illustrates the deterministic solution. Core porosity measurements help cross-check the results.

The bulk modulus and porosity crossplot with the VR bounds are shown in Figure 6. To show effective medium models of a composite rock with more than two constituents on the crossplot, we must group the constituents into two endpoints: generally, the host rock and inclusions (porosity). Therefore, the conventional crossplot cannot (1) present the exact bound values for a composite with more than two constituents and (2) compare effective medium models directly with each log measurement that varies in composition at every depth. Therefore, we present elastic measurements and effective medium models in depth plots.

In this conventional carbonate reservoir, we assume that the host rock is isotropic and compute the VR, SCA, and DEM models from the multimineral result. Track 1 of Figure 7 is the same deterministic result from Figure 5. Tracks 2–5 of Figure 7 illustrate the VR bound models in bulk modulus and P-wave modulus, SCA, and DEM in bulk modulus in separate depth plots.

The VR bound model represents the widest limits, and the effective moduli should fall between them. Thus, most measured bulk modulus values are between the VR bounds. However, there are intervals in which the measured bulk and P-wave modulus are greater or smaller than the limits predicted from the multimineral results. Those violations are colored by flags on the side of each track (Figure 7, tracks 2 and 3). Most of the violations are upper bound violations in intervals with high volumes of anhydrite and low porosity (<5%). Note that the VR bound models in the P-wave modulus show violations relatively consistent with the flags in bulk modulus. Thus, in the absence of an S-wave slowness log, the P-wave modulus may still assist in validating the multimineral results.

For the inclusion models, AR = [0.01, 1] are used for the upper and lower bounds for the SCA and DEM, respectively. Ruiz and Dvorkin (2010) find that a constant of 0.13 for AR can be used to match empirical relations in competent sand, shale, and quartz/calcite mixtures. In addition to the upper and lower bounds, we plot

DOI:10.1190/geo2020-0918.1

calculations of AR = 0.13 for both inclusion models for reference. Track 4 of Figure 7 shows SCA with a narrower distance between upper and lower bounds than the VR bound model. In addition to violation flags determined by the VR bound model, SCA detects more violations, which are not limited to high anhydrite volumes and low-porosity intervals.

In track 5 of Figure 7, DEM shows bulk modulus predictions consistent with SCA. The intermediate DEM (AR = 0.13) exhibits reasonable agreement with the bulk modulus log in low-porosity intervals (<5%). Like SCA, the DEM violations are not limited to high anhydrite volume intervals and include intervals with high porosity (>10%). The underestimate of elastic properties from the SCA and DEM models at high porosity may imply vuggy porosity in the carbonate reservoir. Another plausible reason is that some secondary minerals are not participating in building the rock frame. Geologic information about primary and secondary mineral content would be needed to refine the model further.

As well as the additional geologic information needed for inclusion models, potential causes of the violation in effective medium bounds are tool errors due to borehole roughness (or fractures), incorrect constituents, and inappropriate volume fractions in multimineral analysis. However, there is no fracture around the flagged intervals, according to the wellbore image logs. Caliper and density correction logs indicate that the wellbore in this interval is intact, without obvious roughness. Furthermore, the mud logs confirm the selection of constituents at the flagged intervals. A few violations of the lower limits in all models may be due to the low vertical resolution of the bulk modulus log in alternating thin layers. In the VR bound model, the flagged intervals correspond mostly to the intervals with high anhydrite content and indicate the need to reevaluate the multimineral results. Because the VR bound model defines the extreme limits with no specification in rock texture, we focus on constraining multimineral analysis using the VR bound model in bulk modulus.

The possible reason for the violations in the Voigt average is improper inverted volume fractions. To increase the upper bound in intervals in which violations occur, we need to increase the volume fractions of stiff constituents (dolomite or calcite). To achieve this goal, we impose linear inequality constraints from the VR bounds using the interior-point method (Altman and Gondzio, 1999; The MathWorks, 2018) to find an alternative solution at every depth in the deterministic inversion. The violation of inequality constraints is prevented by augmenting the objective function with a barrier term that causes the optimal solution to be in the feasible space. In addition to equations 6 and 7, the objective function is to find a vector of volume fractions, which minimizes the inverse function, which is subject to linear inequalities at every depth:

$$\begin{bmatrix} K_{\text{sat}} \\ \frac{1}{K_{\text{sat}}} \end{bmatrix} \le \begin{bmatrix} K_1 & K_2 & \cdots & K_i \\ \frac{1}{K_1} & \frac{1}{K_2} & \cdots & \frac{1}{K_i} \end{bmatrix} \begin{bmatrix} m_1 \\ m_2 \\ \vdots \\ m_i \end{bmatrix}, \qquad (12)$$

where K_{sat} is the bulk modulus log. Equation 12 shows the inequality constraints for the VR averages. In this case, the Reuss constraint is not active because the lower bound violations may be due to the difference in vertical resolution between input logs.

The constrained multimineral results are shown in track 2 of Figure 8. For depths with no upper bound violation originally, the results remain unchanged. For depths where the upper bounds were crossed, the constrained inversion uses the bulk modulus log as the upper limit to search for alternative solutions that still honor the input data. Track 3 of Figure 8 shows the new upper bound derived from the alternative solution. The alternative solution shows a reduction of anhydrite by 10%–30% and an increase of calcite or dolomite by the same amount. Tracks 4–8 of Figure 8 show the comparison between the input and reconstructed logs with and without the constraint, and the differences are reasonable, thereby indicating that the alternative solution is plausible.

Calcite, dolomite, and anhydrite are relatively similar in petrophysical endpoints, but they are very different in elastic properties (see Table 1). Using effective medium bounds on the bulk modulus provides a means to reevaluate and constrain the results from multimineral analysis. Unfortunately, there is no core measurement available at those intervals to validate the change of volume fractions from constrained multimineral analysis.

Bakken and Three Forks Formations, North Dakota, USA

Multimineral analysis is especially challenging for unconventional reservoirs due to their complex lithology and uncertainties in petrophysical endpoints. Therefore, we propose to use effective medium models as additional data to quality-control the multimineral results even if there may not be violations in the effective medium model. The second field example is the Bakken and Three Forks formations.

The Three Forks Formation consists of peritidal dolostones and is separated from the overlaying Bakken Formation by a major unconformity. The Bakken Formation is characterized by low-porosity and permeability reservoirs, organic-rich source rocks, and regional hydrocarbon charge. The Bakken Formation consists

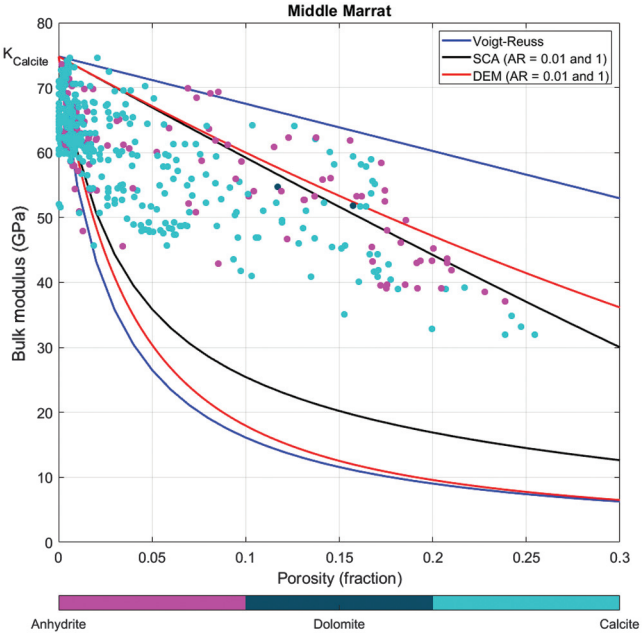

Figure 6. Bulk modulus and porosity crossplot of the Middle Marrat Formation. The Voigt and Reuss averages, SCA, and DEM are calculated from the composite of calcite (K = 74.8 GPa) and the mixture of water and oil (K = 2 GPa). Facies color the data points.

of four members: upper and lower organic-rich black shale called the Lower Bakken Shale (LBSH) and the Upper Bakken Shale (UBS); the oolitic, bioclastic, sandy Middle Member (M. Bakken); and the Pronghorn Formation, a basal member with dolostone, limestone, and siltstone (Sonnenberg, 2017).

The well is in McKenzie County, North Dakota. Available well-log data include GR, RT, RHOB, NPHI, and U for multimineral analysis. The GR measurements include standard (SGR) and computed (CGR, gamma-ray contribution from thorium and potassium) gamma-ray. We only use dipole sonic logs to calculate the bulk modulus log. In addition to logs, XRD data identify quartz, calcite, dolomite, clay, kerogen, and traces of K-feldspar and chlorite for the solid phase. The clay mostly consists of illite. Because of their negligible trace volume fractions, K-feldspar and chlorite are ignored in the multimineral analysis.

Triaxial compressive tests with core plugs that are horizontal, vertical, and 45° to the bedding at various depths are available. With measured bulk densities, the elastic parameters, such as Young's, bulk, and shear moduli, are estimated by the ultrasonic devices under a hydrostatic confining pressure of 15,395 KPa.

For simplicity, we continue to use the linear mixing law (equation 2) for multimineral analysis of the Bakken and Three Forks formations. See Heidari et al. (2012) for a more accurate thinly bedded model using nonlinear equations. Table 3 lists the petrophysical endpoints used in the multimineral analysis. Kerogen is characterized by high GR readings [approximately 3500 American Petroleum Institute (API)] from uranium in the UBS and LBSH.

Figure 9 shows the comparison of the input logs and reconstructed logs from MCMC simulations. Tracks 1–7 of Figure 10 are realizations of constituent volume fractions with uncertainties compared with XRD data. The solution from the deterministic inversion is shown in track 8 of Figure 10. The faithful reconstruction of the input curves and a good match to core data confirm log data quality and consistent model parameterization. Figure 11 shows the bulk modulus crossplotting with porosity. The quartz and carbonate-rich Middle Bakken and Three Forks formations exhibit stiff elastic properties. In contrast, the UBS, LBSH, and Pronghorn show soft elastic properties consisting of more clay and kerogen contents.

The host rock of the Bakken Formation is considered anisotropic (Sayers and Dasgupta, 2015). For proper implementation of SCA and DEM in shales, the model needs to incorporate maturation information while creating the solid. Therefore, we use the VR bound model, which does not require any geometric information of the host rock. Figure 12 shows that the bulk modulus log mostly stays between the VR bounds predicted from the multimineral results. Thus, the solution meets the bound model. There is no need for

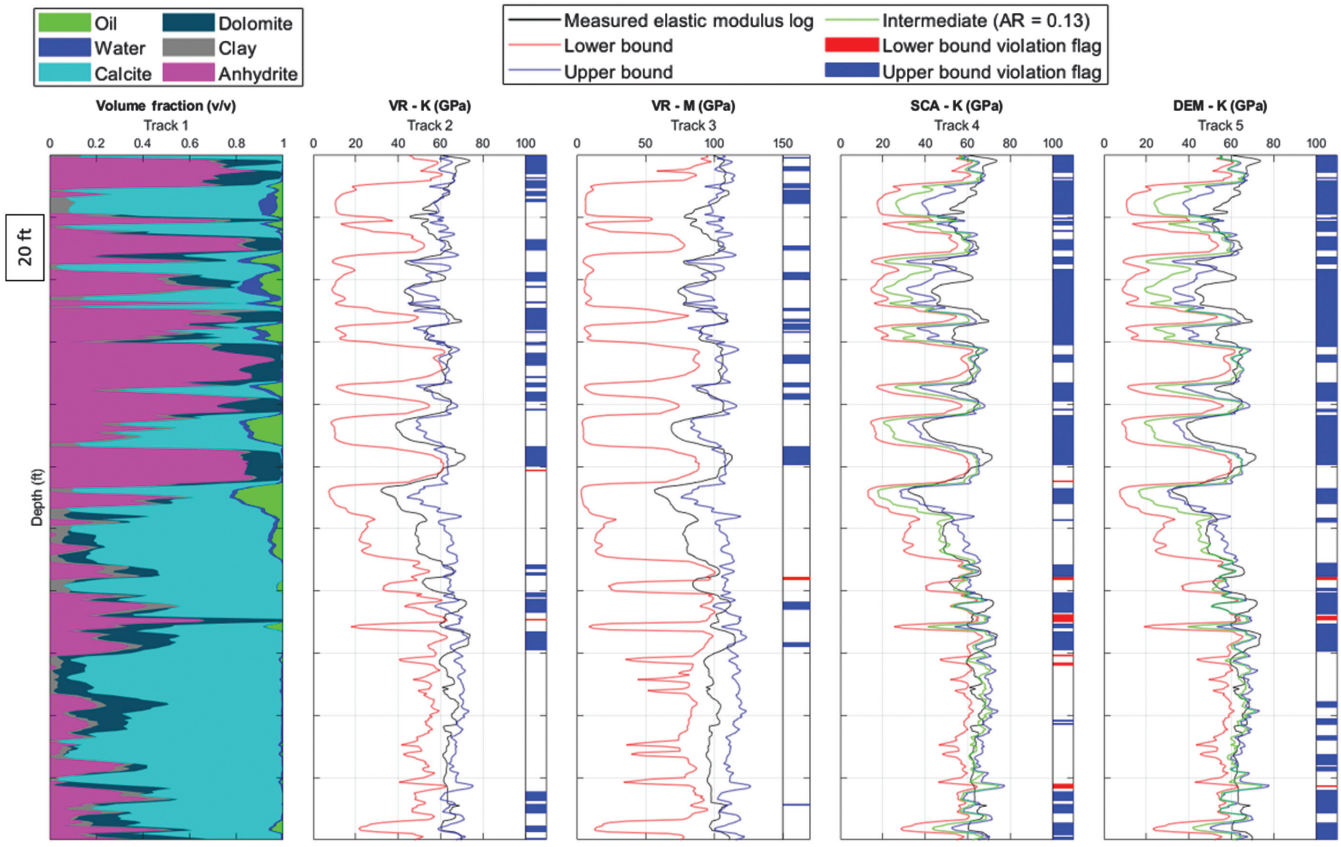

Figure 7. The multimineral results evaluated with effective medium models. Track 1 is the deterministic result from Figure 5. The effective medium models (tracks 2–5) are derived from the multimineral results. Track 2 is the bulk modulus log compared with the VR bound model. Track 3 is the P-wave modulus log compared with the VR bound model in P-wave modulus. Track 4 represents the SCA in bulk modulus with AR = [0.01, 1.0]. Track 5 illustrates the DEM in bulk modulus with AR = [0.01, 1.0]. Intermediate curves are shown for AR = 0.13 for the SCA and DEM. The violations are shown on the side of tracks 2–5 in color flags in which the bulk modulus log is greater than the upper limits (blue) or lower than the lower limits (red) derived from the models.

actively constraining the inversion, except for a few lower bound violations at the boundary of the Middle and LBSH formations, mainly due to the vertical resolution issue. We can still use the VR bound model to validate the multimineral results.

First, the triaxial compressive results can be directly compared with the bounds. The bedding at the wellbore is with near-zero apparent dip. The horizontal plugs measure the bulk modulus parallel to the bedding, whose values should be close to but smaller than the Voigt bound predicted from the multimineral results. Track 2 of Figure 12 shows that all bulk moduli estimated from horizontal plugs are within the predicted Voigt bound, and the measurements at the Pronghorn and Three Forks formations fall close to the bound. Good matches indicate that the solution is plausible.

Second, Simone et al. (2020) analyze the acoustic velocity of core data and provide reference values for the weighting factors of different unconventional reservoirs. The weighting factors for the Bakken Formation are estimated between 0.34 and 0.45. Track 2 of Figure 12 shows two reference curves of weighting factors [0.34, 0.45] compared with the bulk modulus log. The curve of computed weighting factors (equation 11) is shown in track 3 of Figure 12. One may iterate the endpoints or tool responses if the resultant weighting factors are away from the reference. The Middle Bakken Formation is consistent with the suggested range. However, the UBS and LBSH exhibit lower weighting factor values, ranging from 0.15 to 0.25, due to high porosity and high kerogen content. More statistical data are required to have more conclusive estimates on the UBS and LBSH.

Another potential use of the VR bound model is to approximate the local elastic moduli of the clay for unconventional reservoirs. Unlike the well-defined elastic properties of calcite, dolomite,

Table 3. Petrophysical endpoints used for the Bakken and Three Forks Formations.

Constituent	CGR (API)	SGR (API)	Conductivity (S/m)	Density (g/cm^3)	Neutron porosity (fraction)	Volumetric cross section (barns/cm^3)
Quartz	12	15	0	2.65	−0.02	4.8
Calcite	10	15	0	2.71	0	13.7
Dolomite	10	12	0	2.89	0.02	9.0
Clay	260	350	0.1	2.75	0.4	8.7
Kerogen	50	3500	0	1.2	0.5	0.3
Water	0	0	12	1.0	1.0	0.4
Oil	0	0	0	0.8	0.95	0.1

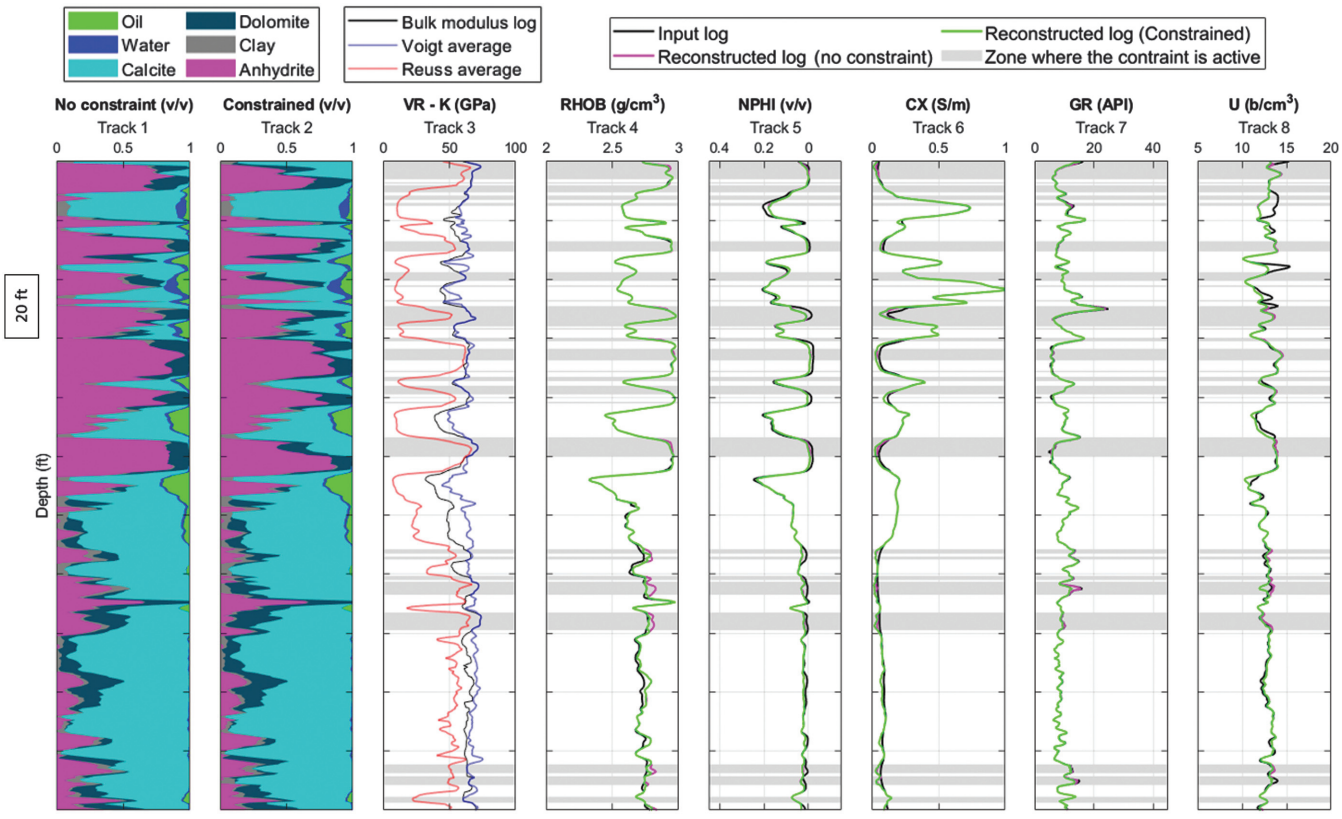

Figure 8. The multimineral results before and after constraint by the VR bound model. Track 1 shows the unconstrained results. Track 2 demonstrates the results constrained by the VR bound model. Track 3 shows the bulk modulus log compared with the effective medium bounds derived from the constrained results. Tracks 4–8 show the input logs, reconstructed logs from unconstrained results, and reconstructed logs from constrained results. Zones where the constraints are active are colored in gray.

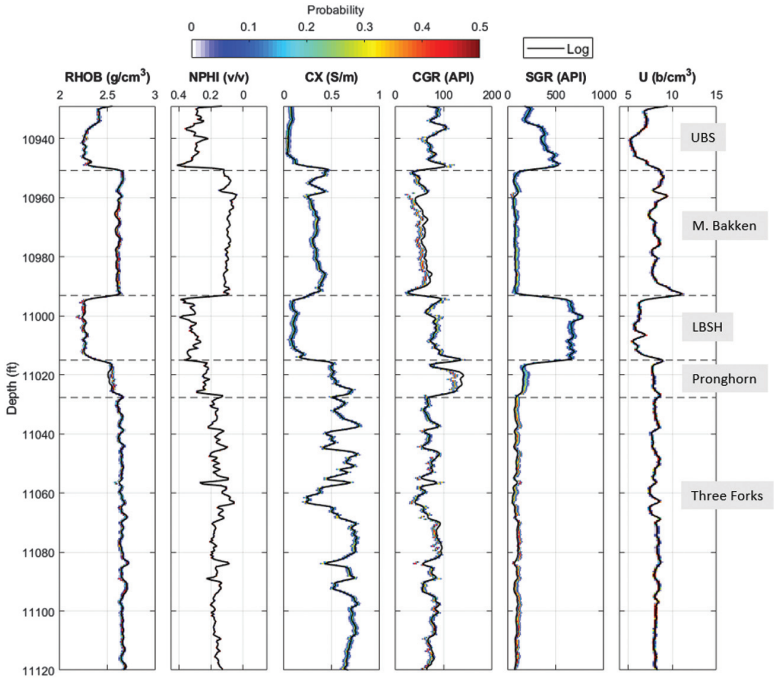

Figure 9. The input logs and reconstructed logs from all of the plausible realizations from MCMC simulations for the Bakken and Three Forks formations. The reconstructed logs are shown as posterior probability functions in colors.

or quartz, clay has high variability in elastic properties due to its complex composition. For example, clay is stiffer when in dryer conditions. Theoretical values for the bulk modulus of clay are reported between 20 and 50 GPa (Wang et al., 2001). Track 2 of Figure 13 shows the VR bounds derived from the multimineral result of the LBSH and Pronghorn formations (Figure 13, track 1) using an initial value of 25 GPa for the dry clay bulk modulus. The predicted Reuss bound of the Pronghorn Formation overlays the bulk modulus log, resulting in close to zero weighting factors. Note that the Reuss bound represents the zero dry bulk modulus according to the Gassmann equation. Such low weighting factor values may result from the incorrect bulk modulus selected for the soft mineral (clay) in the Pronghorn Formation. The reason might be that the clay in the Pronghorn Formation might not have experienced high pressure/temperature to a dryer/stiffer condition. Therefore, we use a lower bulk modulus value of 12 GPa (Vanorio et al., 2003) and recalculate the corresponding VR bounds. Track 3 of Figure 13 shows a more realistic bound model for the Pronghorn Formation

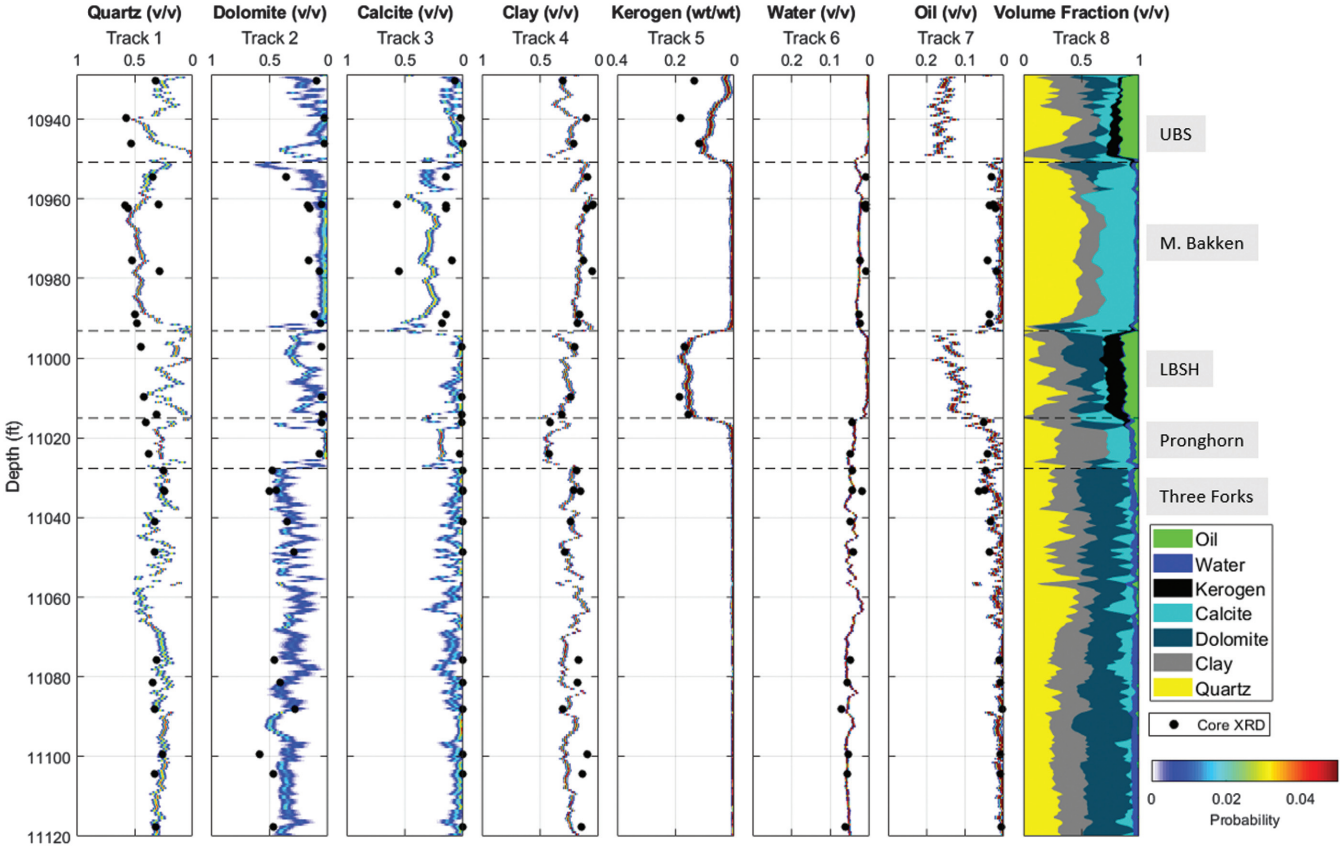

Figure 10. The posterior probability functions of constituent volume fractions (tracks 1–7) from MCMC simulations and the deterministic result (track 8). The core XRD measurements are compared to cross-check the multimineral results.

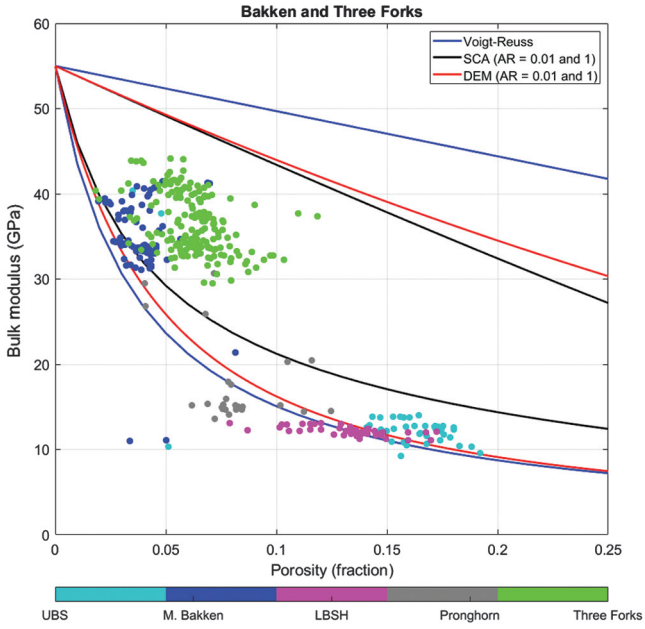

Figure 11. Bulk modulus and porosity crossplot. The data points are colored by formations. The Voigt and Reuss averages, SCA, and DEM are computed from the composite of the matrix (the average of calcite and quartz, K = 55.9 GPa) and the mixture of water and oil (K = 2 GPa).

and indicates that a lower clay bulk modulus value should be used. The method is most useful when the intervals contain a high volume of clay minerals.

DISCUSSION

We implement the effective medium theory using quad-combo logging data to evaluate multimineral models. In addition to the conventional elastic moduli-porosity crossplot, depth plot is recommended to facilitate a more accurate and intuitive comparison among the measured bulk modulus, the variation in rock composition, and the bounds derived from theoretical effective medium models.

Three effective medium models are computed from the multimineral results and compared. The VR bound model represents the most extreme theoretical limits for effective moduli of a saturated rock. If there are violations of the VR bound model, it indicates the need to reevaluate the multimineral result. The SCA and DEM narrow the range of plausible effective moduli by specifying the AR. Our experiment in the MMR case shows that AR = [0.01, 1.0] of SCA and DEM are realistic upper and lower bounds for a low-porosity approximation. However, for porous intervals, a more accurate approximation is required. SCA and DEM may be adequate for quality control purposes. Still, without additional geologic information about load-bearing versus nonload-bearing minerals, the bounds might not be calculated properly to constrain multimineral results.

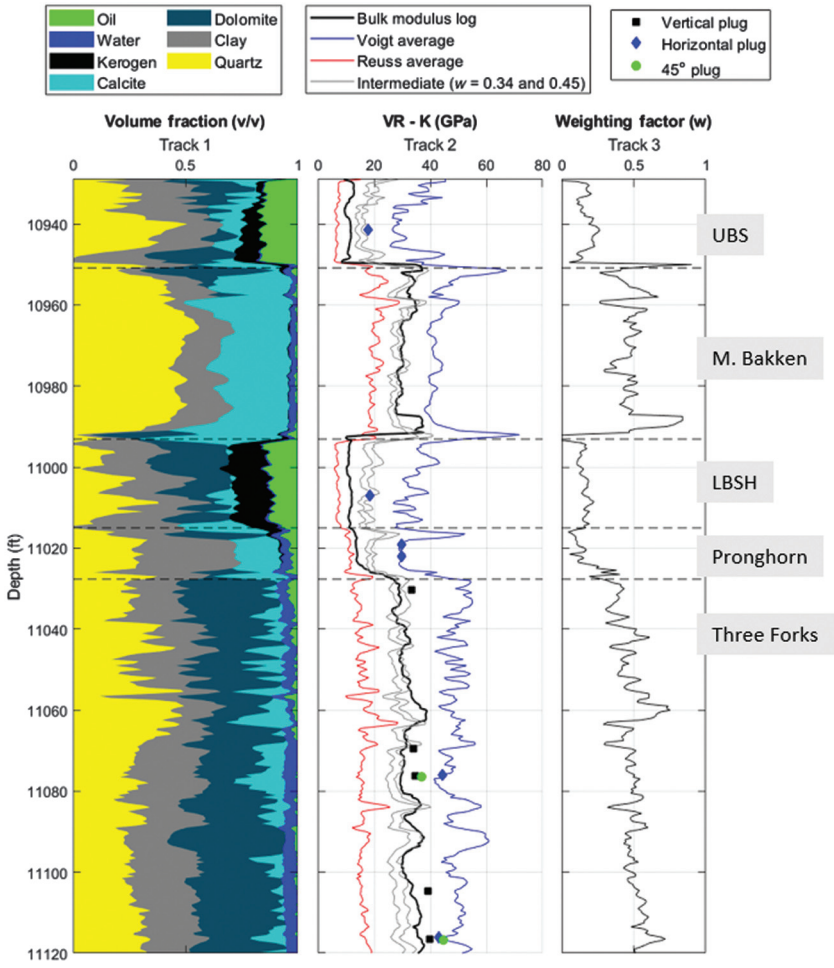

Figure 12. The weighting factor evaluation for the Bakken and Three Forks formations. Track 1 shows the deterministic results from Figure 10. Track 2 shows the bulk modulus log compared with the VR bound model computed from track 1 and the triaxial test results. The intermediate reference curves (w = [0.34, 0.45]; Simone et al., 2020) for the Bakken Formation are plotted. The weighting factor curve is shown in track 3.

DOI:10.1190/geo2020-0918.1

The VR bound model violations indicate that errors may have occurred in selecting constituents, estimated composition, or other reasons (e.g., due to tool errors or borehole issues). For the MMR case, the MCMC simulations show high uncertainties in calcite and anhydrite volume fractions. The violation of the VR bound model most likely occurs in which the petrophysical endpoints of constituents are similar, but the constituents are distinct in terms of their elastic properties. Therefore, one may use the constraints to the inverse problem within the feasible area in the model space to find an alternative solution that honors the input logs. Such inequality constraints can be easily implemented in commercial software. Using the VR bound model, the P-wave modulus is another viable option when the DTS log is absent or too noisy.

Even if there is no violation in the VR bound model, estimating the weighting factor (w) can be useful for quality control of multimineral results and the approximation for elastic moduli of constituents. The change in the weighting factor along the depth may represent the difference in the geometry of the rock. When the weighting factor is between zero and one, the value of the weighting curve may be used to inspect the results at different levels, especially for formations that already have a range of weighting factors estimated from laboratory experiments or a set of offset wells. For example, the Middle Bakken and Three Forks formations exhibit stiffer elastic properties, with w ranging from 0.34 to 0.45. However, the UBS and LBSH are softer, with w ranging from 0.15 to 0.25. The findings still require more statistical evaluation. Analyzing the weighting factor also helps approximate the elastic properties of minerals such as clay that have variability due to their complex mineralogy.

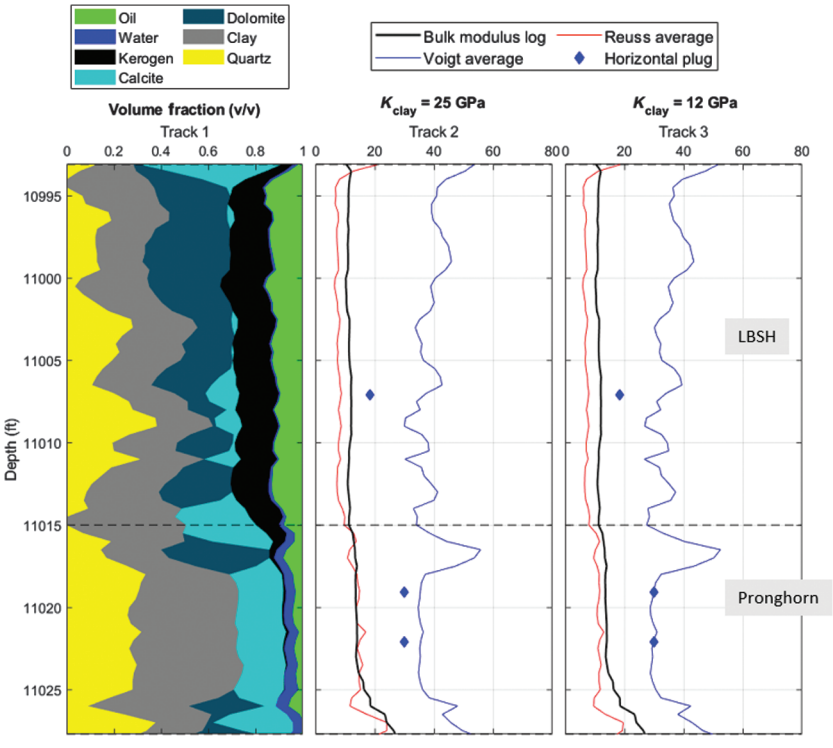

Figure 13. Iterative tests for the approximation of the clay bulk modulus. Track 1 is the multimineral result. The K_{clay} = 25 GPa is used for the VR bound shown in track 2. Track 3 shows the VR bound with K_{clay} = 12 GPa.

The VR bound model accommodates the most extreme cases in completely layered formations (Sone and Zoback, 2013). Therefore, our bound model method applies to rocks with isotropic and transversely isotropic elastic properties. We recommend computing the VR bounds simultaneously and comparing the bulk modulus log, core measurements, and bounds after every iteration of multimineral analysis. Results of triaxial compressive tests may be directly compared on the depth plot to assist multimineral interpretation. However, note that we use the isotropic approximation (equation 8) to compute the bulk modulus log due to the common limitation of well-log data. The weighting factor variation along the depth and between different wells may result from the rock texture and anisotropy for transversely isotropic rocks. More studies are required to understand the effects of anisotropic properties under the isotropic assumption.

CONCLUSION

We present a study of implementing effective medium models in multimineral analysis. Among the models tested in this paper, the VR bound model is more practical than inclusion models and can be the first-order quality control for multimineral analysis. If violations are present, one may impose inequality constraints to seek an alternative solution after ruling out other possible causes. Linear interpolation between the VR bounds may help guide multimineral analysis for unconventional reservoirs. The new method provides a means to incorporate rock physics in multimineral analysis in addition to empirical slowness/velocity relations.

ACKNOWLEDGMENTS

The authors thank Kuwait Oil Company and the Ministry of Oil, the State of Kuwait, for granting permission to publish this paper. The authors are indebted to Chris Skelt, two other anonymous reviewers, and editors for their constructive discussion and comments on the manuscript. We also thank members of the Reservoir Characterization Project (RCP) at the Colorado School of Mines for their financial support and Patricia Rodrigues for her help finding the Bakken data set.

DATA AND MATERIALS AVAILABILITY

Data associated with this research are confidential and cannot be released.

APPENDIX A

BAYESIAN INVERSION FOR MULTIMINERAL ANALYSIS

Due to data errors and uncertainties in petrophysical endpoints, assessing the uncertainty of multimineral analysis is critical. The conventional linear solvers can only optimize the inverse problem for limited solutions and do not provide uncertainties of volume fractions in the analysis.

The MCMC simulations in the Bayesian framework allow us to propagate the uncertainty from data and formula to the estimated multimineral result. We can use the estimated posterior probability functions to evaluate the uncertainties. For a given data set (D), the posterior probability function $p(m|D)$ of the model parameter m can be sampled from

$$p(m|D) \propto p(D|m)p(m), \tag{A-1}$$

where $p(D|m)$ is the likelihood function and $p(m)$ is the prior distribution of the model parameter. For multimineral analysis, m represents a vector of volume fractions of constituents. We assume the linear mixing law for multimineral analysis (equation 2). The likelihood function $p(D|m)$ can be described by

$$p(D|m) \propto \exp\left[-\frac{1}{2}(Gm - D)^T W^{-1}(Gm - D)\right], \tag{A-2}$$

where W is a diagonal matrix containing terms related to the weighting of well logs. The unity equation is one of the constraining equations to ensure material balance.

There are two main sources of uncertainties in the multimineral analysis. The primary uncertainty comes from data errors. After determining the acceptable data misfits, MCMC simulations aim to search the model space and produce posterior probability functions within the targeted data misfit. The secondary uncertainty results from the similarity in constituent endpoints. Even when the inverse problem is well determined (the number of logs plus the unity constraint is equal to or greater than the number of unknown volume fractions), the uncertainty of each constituent volume fraction is different. In this paper, the posterior probability distributions of constituent volume fractions are displayed as color schemes at every depth.

NOMENCLATURE

CX	=	Near-wellbore square root conductivity log
d	=	Vector of well-log data
DTC	=	Compressional slowness log
DTS	=	Shear slowness log
GR	=	Gamma-ray log
G	=	Matrix of constituent petrophysical endpoints
RT	=	Ture formation resistivity log
ρ_b	=	Bulk density log
ϕ_N	=	Neutron porosity log
ϕ	=	Total porosity
m	=	Vector of constituent volume fractions
m_i	=	Volume fraction of the ith constituent
M	=	Number of independent log curves
N	=	Number of unknown constituent volume fractions
LDT	=	Litho-density tool
M_{sat}	=	P-wave modulus of a saturated rock
K	=	Bulk modulus
K_{sat}	=	Bulk modulus of a saturated rock
K_R	=	Reuss average
K_V	=	Voigt average
PEF	=	Photoelectric absorption factor log as a massic cross section
V_{P}	=	P-wave velocity
V_{S}	=	Shear-wave velocity
w	=	Weighting factor
U	=	Volumetric cross section
XRD	=	X-ray diffraction
XRF	=	X-ray fluorescence

REFERENCES

Alsharhan, A. S., C. J. Strohmenger, F. H. Abdullah, and G. Al Sahlan, 2014, Mesozoic stratigraphic evolution and hydrocarbon habitats of Kuwait, *in* L. Marlow, C. Kendall, and L. Yose, eds., Petroleum systems of the Tethyan region: AAPG Memoir, **106**, 541–611.

Altman, A., and J. Gondzio, 1999, Regularized symmetric indefinite systems in interior point methods for linear and quadratic optimization: Optimization Methods and Software, **11**, 275–302, doi: 10.1080/10556789908805754.

Archie, G. E., 1942, The electrical resistivity log as an aid in determining some reservoir characteristics: Transactions of the American Institute of Mining, Metallurgical, and Petroleum Engineers, **146**, 54–62.

Berryman, J. G., 1980, Long-wavelength propagation in composite elastic media: Journal of the Acoustic Society of America, **68**, 1809–1819, doi: 10.1121/1.385171.

Berryman, J. G., S. R. Pride, and H. F. Wang, 2002, A differential scheme for elastic properties of rocks with dry or saturated cracks: Geophysical Journal International, **151**, 597–611, doi: 10.1046/j.1365-246X.2002.01801.x.

Carmichael, R. S., 1989, Practical handbook of physical properties of rocks and minerals: CRC Press.

Dandekar, D. P., 1986, Pressure dependence of the elastic constants of calcite: Physical Review, **172**, 873, doi: 10.1103/PhysRev.172.873.

Das, A., and M. Batzle, 2009, A combined effective medium approach for modeling the viscoelastic properties of heavy oil reservoirs: 79th Annual International Meeting, SEG, Expanded Abstracts, 2110–2114, doi: 10.1190/1.3255273.

Doveton, J. H., 1994, Geologic log analysis using computing methods: AAPG, AAPG Studies in Geology **2**.

Dvorkin, J., and A. Nur, 1998, Time-average equation re-visited: Geophysics, **63**, 460–464, doi: 10.1190/1.1444347.

Hashin, Z., and S. Shtrikman, 1963, A variational approach to the elastic behavior of multiphase materials: Journal of the Mechanical Physics of Solids, **11**, 127–140, doi: 10.1016/0022-5096(63)90060-7.

Heidari, Z., C. Torres-Verdín, and W. E. Preeg, 2012, Improved estimation of mineral and fluid volumetric concentrations from well logs in thinly bedded and invaded formations: Geophysics, **77**, no. 3, WA79–WA98, doi: 10.1190/geo2011-0454.1.

Hill, R., 1952, The elastic behavior of crystalline aggregate: Proceeding of Physical Society, London, **65**, 349–354, doi: 10.1088/0370-1298/65/5/307.

Hill, R., 1964, Theory of mechanical properties of fibre-strengthened materials — I: Elastic behaviour: Journal of the Mechanics and Physics of Solids, **12**, 199–212, doi: 10.1016/0022-5096(64)90019-5.

Humbert, P., and F. Plieque, 1972, Propriétés élastiques de carbonates rhomboédriques monocristillins: Calcite, magnésite, dolomite: Comptes Rendues de l'Academie Sciences Paris, **275**, 391–394.

King, M. S., 1969, Static and dynamic elastic moduli of rocks under pressure: Proceedings of the 11th U.S. Symposium on Rock Mechanics, 329–351.

Kittridge, M. G., 2014, Investigating the influence of mineralogy and pore shape on the velocity of carbonate rocks: Insights from extant global data sets: Presented at the 55th Annual Logging Symposium, SPWLA.

Marion, D., and A. Nur, 1991, Pore-filling material and its effect on velocity in rocks: Geophysics, **56**, 225–230, doi: 10.1190/1.1443034.

Mavko, G., T. Mukerji, and J. Dvorkin, 2009, The rock physics handbook: Cambridge University Press.

Mayer, C., and A. Sibbit, 1980, Global, a new approach to computer-processed log interpretation: 55th Annual Technical Conference and Exhibition, SPE, Extended Abstracts, SPE-9341-MS, doi: 10.2118/9341-MS.

Michelena, R. J., K. S. Godbey, M. J. Uland, and P. E. Rodrigues, 2020, Petrophysical multimineral analysis using genetic optimization to solve complex mineral composition in unconventional reservoirs: 90th Annual International Meeting, SEG, Expanded Abstracts, 2455–2463, doi: 10.1190/segam2020-3425780.1.

Mitchell, W. K., and R. J. Nelson, 1988, A practical approach to statistical log analysis: Presented at the 29th Annual Logging Symposium, SPWLA.

Murris, R. J., 1980, Middle East: Stratigraphic evolution and oil habitat: Bulletin of the American Association of Petroleum Geologists, **4**, 597–618, doi: 10.1306/2F918A8B-16CE-11D7-8645000102C1865D.

Quirein, J., S. Kimminau, J. LaVigne, J. Singer, and F. Wendel, 1986, A coherent framework for developing and applying multiple formation evaluation models: Presented at the 27th Annual Logging Symposium, SPWLA.

Rabaute, A., A. Revil, and E. Brosse, 2003, In situ mineralogy and permeability logs from downhole measurements: Application to a case study in clay-coated sandstone formations: Journal of Geophysical Research, **108**, 1–16, doi: 10.1029/2002JB002178.
Rafavich, F., C. H. St, C. Kendal, and T. P. Todd, 1984, The relationship between acoustic properties and the petrographic character of carbonate rocks: Geophysics, **49**, 1622–1636, doi: 10.1190/1.1441570.
Raymer, L. L., E. R. Hunt, and J. S. Gardner, 1980, An improved sonic transit time-to-porosity transform: Presented at the 21st Annual Logging Symposium, SPWLA.
Reuss, A., 1929, Berechnung der Fließgrenze von Mischkristallen auf Grund der Plastizitätsbedingung für Einkristalle: Zeitschrift Für Angewandte Mathematik Und Physik, **9**, 49–58, doi: 10.1002/zamm.19290090104.
Ruiz, F., and J. Dvorkin, 2010, Predicting elasticity in nonclastic rocks with a differential effective medium model: Geophysics, **75**, no. 1, E41–E53, doi: 10.1190/1.3267854.
Saxena, A., M. Krief, and L. Adam, 2018, Handbook of borehole acoustics and rock physics for reservoir characterization: Elsevier Science.
Sayers, C. M., and S. Dasgupta, 2015, Elastic anisotropy of the Middle Bakken Formation: Geophysics, **80**, no. 1, D23–D29, doi: 10.1190/geo2014-0219.1.
Simone, A., L. Hathon, and M. Myers, 2020, Acoustic velocity modeling of unconventional reservoirs: Unconventional Resources Technology Conference, SEG, Global Meeting Abstracts, 307–324, doi: 10.15530/urtec-2020-2667.
Sone, H., and M. D. Zoback, 2013, Mechanical properties of shale-gas reservoir rocks — Part 1: Static and dynamic elastic properties and anisotropy: Geophysics, **78**, no. 5, D381–D392, doi: 10.1190/geo2013-0050.1.
Sonnenberg, S., 2017, Sequence stratigraphy of the Bakken and Three Forks Formations, Williston Basin, USA: AAPG Search and Discovery Article #10990.
The MathWorks, 2018, Optimization toolbox: The MathWorks.
Vanorio, T., M. Prasad, and A. Nur, 2003, Elastic properties of dry clay mineral aggregates, suspensions and sandstones: Geophysical Journal International, **155**, 319–326, doi: 10.1046/j.1365-246X.2003.02046.x.
Voigt, W., 1889, Ueber die Beziehung zwischen den beiden Elastizita tskonstanten isotroper Korper: Annalen der Physik, **38**, 573–587, 10.1002/andp.18892741206.
Walker, K., Q. Sun, and R. Wang, 2019, Wavelength-based axial resolution limitations of flexural wave dispersion sonic logging: Presented at the 60th Annual Logging Symposium, SPWLA.
Wang, Z., H. Wang, and M. E. Cates, 2001, Effective elastic properties of solid clays: Geophysics, **66**, 428–440, doi: 10.1190/1.1444934.
Wood, A. W., 1955, A textbook of sound: McMillan Co.
Wyllie, M. R. J., A. R. Gregory, and L. W. Gardner, 1956, Elastic wave velocities in heterogeneous and porous media: Geophysics, **21**, 41–70, doi: 10.1190/1.1438217.
Yan, F., and D. H. Han, 2013, Measurements of elastic properties of kerogen: 83rd Annual International Meeting, SEG, Expanded Abstracts, 2778–2782, doi: 10.1190/segam2013-1319.1.
Zimmerman, R. W., 1990, Compressibility of sandstones: Elsevier Science.

Biographies and photographs of the authors are not available.